

Photocytotoxic ferrocene-appended (L-tyrosine)copper(II) complexes of phenanthroline bases

Tridib K. Goswami^a, Sudarshan Gadadhar^b, Anjali A. Karande^{b,*}, Akhil R. Chakravarty^{a,*}

^a Department of Inorganic and Physical Chemistry, Indian Institute of Science, Sir C.V. Raman Avenue, Bangalore 560012, India

^b Department of Biochemistry, Indian Institute of Science, Sir C.V. Raman Avenue, Bangalore 560012, India

ARTICLE INFO

Article history:

Available online 18 June 2012

Dedicated to Alfred Werner on the 100th Anniversary of his Nobel prize in chemistry in 1913.

Keywords:

Ferrocene
Copper
Crystal structure
DNA Photocleavage
Photocytotoxicity
Cellular imaging

ABSTRACT

Copper(II) complexes of ferrocene(Fc)-conjugated reduced Schiff base of L-tyrosine (Fc-TyrH), viz., [Cu(Fc-Tyr)(L)](ClO₄), where L is 1,10-phenanthroline (phen, **1**), dipyrido[3,2-d:2',3'-f]quinoxaline (dpq, **2**), dipyrido[3,2-a:2',3'-c]phenazine (dppz, **3**) and 2-(naphthalen-1-yl)-1H-imidazo[4,5-f][1,10]phenanthroline (nip, **4**), were prepared and tested for their photocytotoxicity in cancer cells. [Cu(Fc-Phe)(phen)](ClO₄) (**5**) of L-phenylalanine and [Cu(Ph-Tyr)(L)(ClO₄)] of the reduced Schiff base Ph-TyrH derived from benzaldehyde and L-tyrosine having phen (**6**) and dppz (**7**), and [Cu(Ph-Phe)(phen)(ClO₄)] (**8**) using L-phenylalanine were prepared and used as controls. Complexes **5** and **6** were structurally characterized by X-ray crystallography. A copper(II)-based d–d band near 600 nm and a ferrocenyl band at ~450 nm were observed in DMF–Tris–HCl buffer (1:4 v/v) in respective complexes. The complexes are photocleavers of pUC19 DNA in visible light forming •OH radicals. They are cytotoxic in HeLa (human cervical cancer) and MCF-7 (human breast cancer) cells showing an enhancement of cytotoxicity in visible light. Fluorescence imaging shows nuclear localization of the complexes.

© 2012 Elsevier Ltd. All rights reserved.

1. Introduction

Metal complexes have been extensively studied for their various therapeutic applications [1–5]. Among them, cisplatin and its analogues are found to show anticancer activity against different cancer cell lines [1,6–9]. The dark toxicity and poor selectivity are generally the major issues for the failure and limitations of the platinum(II) based chemotherapeutic drugs. This has led to the discovery of platinum(IV) prodrugs which can be activated in the cancer cells by chemical or photochemical means [10–14]. Cytotoxicity resulting from photoactivation of the prodrugs which are otherwise non-toxic to the cells in dark is an attractive possibility to circumvent the toxicity associated with the chemotherapeutic drugs [15–21]. Photodynamic therapy (PDT) has received significant current attentions due to its non-invasive nature, reduced side effects and for its selective action on the tumour leaving unexposed healthy cells unaffected [15–18]. The porphyrin-based PDT agents show skin sensitivity and hepato-toxicity [22,23]. This has prompted search for metal-based PDT agents as photosensitizers [24–28]. Sadler and co-workers reported a Pt(IV)-azido prodrug which on photoexcitation generates the active species which is active against a number of cell lines in *in-vitro* studies, significantly

against cisplatin resistant cell line A2780 [29]. Among the metal-based PDT agents, 3d and 4d metal complexes are reported to show photocytotoxicity in visible light [21,24–35]. Unlike the organic PDT agents, the redox active metal complexes are known to show generation of hydroxyl radicals as the reactive oxygen species (ROS) by a photo-redox pathway [36,37].

The present work stems from our interests to develop the chemistry of ferrocene-conjugated copper(II) complexes as potential photocytotoxic agents in visible light [38–40]. The utility of ferrocene-appended breast cancer drug tamoxifen, commonly known as ferrocifen, is well known against both hormone dependent and independent cases while tamoxifen is inactive for the hormone independent ones [41]. This augmentation in the activity of ferrocifen is attributed to the reversible redox chemistry of ferrocene [42,43]. Again, the anti-malarial activity of chloroquine gets enhanced on attaching the ferrocene moiety to the parent drug [44]. Besides the ferrocene-conjugates, several half-sandwich arene-metal complexes are known to show prominent anticancer activity, particularly for metastatic cancer cells [45–47]. The chemistry of organometallic PDT agents showing photocytotoxicity in visible light is relatively new. While organometallic complexes of Fe and W are known to show DNA cleavage activity in high power UV-A light, the ferrocene-conjugated copper(II) and oxovanadium(IV) complexes display photodynamic effect in HeLa and MCF-7 cell lines in visible light [38–40,48–52]. Porphyrin-conjugated (arene)ruthenium(II) complexes are reported to show PDT

* Corresponding authors. Fax: +91 80 23601552.

E-mail addresses: anjali@biochem.iisc.ernet.in (A.A. Karande), arc@ipc.iisc.ernet.in (A.R. Chakravarty).

activity due to the presence of a porphyrin moiety which acts as a photosensitizer [53,54].

Herein, we present the synthesis, characterization, DNA binding, photo-enhanced DNA cleavage activity and photocytotoxic properties of four ferrocene-appended reduced Schiff base (Fc-TyrH) copper(II) complexes of L-tyrosine and phenanthroline bases, viz., [Cu(Fc-Tyr)(L)](ClO₄), where L is 1,10-phenanthroline (phen in **1**), dipyrido[3,2-d:2',3'-f]quinoxaline (dpq in **2**), dipyrido[3,2-a:2',3'-c]phenazine (dppz in **3**) and 2-(naphthalen-1-yl)-1H-imidazo[4,5-f][1,10]phenanthroline (nip in **4**) (Fig. 1). The (1,10-phenanthroline)copper(II) complex of the reduced Schiff base derived from L-phenylalanine and ferrocenecarboxaldehyde, viz., [Cu(Fc-Phe)(phen)](ClO₄) (**5**) is prepared, structurally characterized and evaluated for its biological potential to explore the effect of the ferrocene moiety in this series of complexes. Complexes [Cu(Ph-Tyr)(L)](ClO₄), where L is phen (in **6**) and dppz (in **7**) and Ph-TyrH is the reduced Schiff base of benzaldehyde and L-tyrosine, and [Cu(Ph-Phe)(phen)](ClO₄) (**8**), where Ph-Phe is the reduced Schiff base of L-phenylalanine and benzaldehyde are prepared and used as control species to study the visible light-induced cytotoxicity in HeLa and MFC-7 cancer cell lines (Fig. 1). Significant results of this study are the enhanced activity in the DNA photocleavage and photocytotoxicity of the ferrocene-appended complexes compared to the controls which lack the ferrocenyl moiety. Complex **4** with a pendant naphthyl fluorophore is used to study the cellular uptake. The fluorescence microscopic images showed significant nuclear localization of complex **4** in HeLa cells.

2. Experimental

2.1. Materials and measurements

All the reagents and chemicals were obtained from commercial sources (s.d. Fine Chemicals, India; Sigma–Aldrich, USA) and used as such. Solvents used were purified by reported procedures [55]. Supercoiled pUC19 DNA (cesium chloride purified) was purchased from Bangalore Genie (India). Tris-(hydroxymethyl)aminomethane–HCl (Tris–HCl) buffer solution was prepared using deionized and sonicated triple distilled water. Calf thymus (ct) DNA, agarose

(molecular biology grade), distamycin, methyl green, KI, catalase, NaN₃, L-histidine, SOD (superoxide dismutase), 2,2,6,6-tetramethyl-4-piperidone (TEMP), acridine orange (AO), ethidium bromide (EB), bromophenol blue, xylene cyanol, Dulbecco's Modified Eagle's Medium (DMEM), propidium iodide (PI) and MTT (3-(4,5-dimethylthiazol-2-yl)-2,5-diphenyltetrazolium bromide) were purchased from Sigma (USA). Dipyrido[3,2-d:2',3'-f]quinoxaline (dpq) and dipyrido[3,2-a:2',3'-c]phenazine (dppz) were prepared by reported procedures using 1,10-phenanthroline-5,6-dione as a precursor reacted with ethylenediamine and 1,2-phenylenediamine, respectively [56,57]. 2-(Naphthalen-1-yl)-1H-imidazo[4,5-f][1,10]phenanthroline (nip) was prepared following literature procedure using 1,10-phenanthroline-5,6-dione and 1-naphthaldehyde [58]. Fc-TyrH was prepared according to a literature procedure [59].

The elemental analysis was carried out using a Thermo Finnigan Flash EA 1112 CHN analyzer. The infrared, UV–Vis and emission spectra were recorded on PerkinElmer Lambda 35, PerkinElmer Spectrum one 55 and PerkinElmer LS 55 spectrophotometer, respectively. Molar conductivity measurements were performed using a Control Dynamics (India) conductivity meter. Room temperature solution state magnetic susceptibilities of the copper(II) complexes in DMSO-*d*₆ containing 1% TMS (v/v) as the internal reference were obtained by Evans method using Bruker AMX-400 NMR spectrometer [60,61]. The magnetic moments were calculated using the equation: $\mu_{\text{eff}} = 0.0618(\Delta f/T/fM)$, where Δf is the observed shift in frequency of the TMS signal, T is the temperature (K), f is the operating frequency (MHz) of the NMR spectrometer, and M is the molarity of the complex in the solution. Cyclic voltammetric measurements were carried out at 25 °C on a EG&G PAR Model 253 VersaStat potentiostat/galvanostat using a three electrode set-up with a glassy carbon working, platinum wire auxiliary and a saturated calomel reference (SCE) electrode. Tetrabutylammonium perchlorate (TBAP) (0.1 M) was used as a supporting electrolyte in DMF. The electrochemical data were uncorrected for junction potentials. ¹H NMR spectra were recorded at room temperature on a Bruker 400 MHz NMR spectrometer. Electrospray ionization mass spectral measurements were done using Esquire 3000 plus ESI (Bruker Daltonics) Spectrometer. Fluorescence microscopic investigations were carried out on fluorescence microscope (Carl Zeiss, Germany) using an oil immersion lens.

2.2. Synthesis

2.2.1. Preparation of [Cu(Fc-Tyr)(L)](ClO₄) (L = phen, **1**; dpq, **2**; dppz, **3**; nip, **4**)

Complexes **1–4** were prepared by a general synthetic procedure in which a 0.2 g (1.0 mmol) quantity of copper(II) acetate hydrate in 15 mL aqueous methanol (1:1 v/v) was reacted with the heterocyclic base (L: phen, 0.19 g; dpq, 0.23 g; dppz, 0.29 g; nip, 0.35 g, 1.0 mmol) while stirring at room temperature for 0.5 h followed by addition of solid Fc-TyrH (1.0 mmol, 0.38 g) in small portions with continuous stirring. The reaction mixture was stirred for 1.5 h, and the product was isolated as a green solid in ~70% yield on addition of a methanol solution of NaClO₄ (1.0 mmol, 0.12 g). The solid was isolated, washed with water and cold methanol followed by drying in vacuum over P₄O₁₀ (Yield: 0.53 g, 74% for **1**; 0.55 g, 71% for **2**; 0.56 g, 68% for **3**; 0.61 g, 69% for **4**).

Anal. Calc. for C₃₂H₂₈N₃O₇ClFeCu (**1**): C, 53.28; H, 3.91; N, 5.82. Found: C, 53.09; H, 3.88; N, 5.91%. Selected IR data (cm⁻¹): 3220br, 2155w, 2076w, 2015w, 1630vs (COO_{asym}), 1517s, 1430s, 1370m (COO_{sym}), 1253m, 1096vs (ClO₄⁻), 916w, 842s, 720s, 621s, 555w, 484s, 429w. (vs, very strong; s, strong; m, medium; w, weak; br, broad). ESI-MS in MeOH: *m/z* 621 [M–(ClO₄⁻)]⁺. UV–Vis in DMF–Tris–HCl buffer (1:4 v/v) [λ_{max} /nm (ϵ /M⁻¹ cm⁻¹): 590 (119), 440 (297), 272 (28125), 295sh (9075) (sh, shoulder). $\mu_{\text{eff}} = 1.80 \mu_{\text{B}}$ at

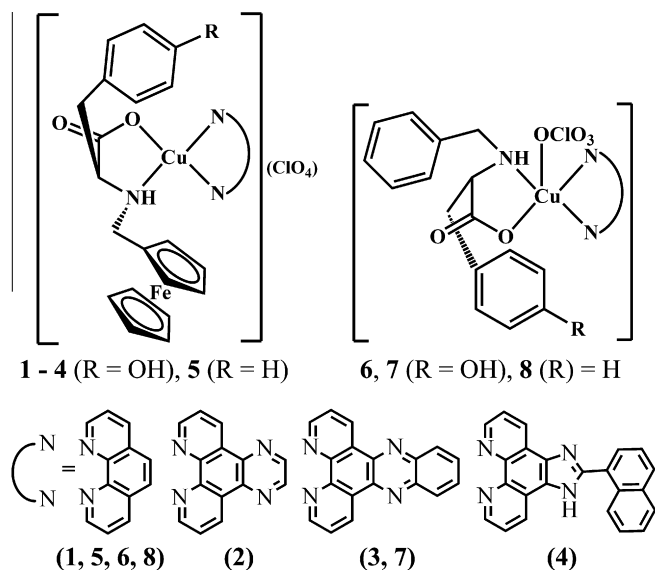


Fig. 1. Schematic drawings of the complexes [Cu(Fc-Tyr)(L)](ClO₄) (L = phen, **1**; dpq, **2**; dppz, **3**; nip, **4**), [Cu(Fc-Phe)(phen)](ClO₄) (**5**), [Cu(Ph-Tyr)(L)](ClO₄) (L = phen, **6**; dppz, **7**) and [Cu(Ph-Phe)(phen)](ClO₄) (**8**) and the heterocyclic bases used.

298 K in DMSO-*d*₆ containing 1% TMS (v/v). $\Lambda_M = 79 \text{ S m}^2 \text{ M}^{-1}$ in DMF at 25 °C.

Anal. Calc. for C₃₄H₂₈N₅O₇ClFeCu (**2**): C, 52.80; H, 3.65; N, 9.05. Found: C, 52.62; H, 3.65; N, 9.19%. Selected IR data (cm⁻¹): 3235br, 3085w, 2995w, 2080w, 2012w, 1636vs (COO_{asym}), 1512m, 1485w, 1447w, 1383s (COO_{sym}), 1238m, 1086vs (ClO₄⁻), 920w, 814s, 726s, 620s, 556w, 485s, 436m. ESI-MS in MeOH: *m/z* 673 [M-(ClO₄⁻)]⁺. UV-Vis in DMF-Tris-HCl buffer (1:4 v/v) [$\lambda_{\text{max}}/\text{nm}$ ($\epsilon/\text{M}^{-1} \text{ cm}^{-1}$)]: 595 (123), 452 (298), 337 (4050), 323 (66650), 298sh (13925), 258 (41650). $\mu_{\text{eff}} = 1.81 \mu_B$ at 298 K in DMSO-*d*₆ containing 1% TMS (v/v). $\Lambda_M = 82 \text{ S m}^2 \text{ M}^{-1}$ in DMF at 25 °C.

Anal. Calc. for C₃₈H₃₀N₅O₇ClFeCu (**3**): C, 55.42; H, 3.67; N, 8.50. Found: C, 55.18; H, 3.38; N, 8.20%. Selected IR data (cm⁻¹): 3450br, 3240w, 2925w, 2015w, 1638vs (COO_{asym}), 1497s, 1419s, 1355s (COO_{sym}), 1235 m, 1075vs (ClO₄⁻), 817s, 764s, 726s, 620s, 487m, 424m. ESI-MS in MeOH: *m/z* 723 [M-(ClO₄⁻)]⁺. UV-Vis in DMF-Tris-HCl buffer (1:4 v/v) [$\lambda_{\text{max}}/\text{nm}$ ($\epsilon/\text{M}^{-1} \text{ cm}^{-1}$)]: 585 (129), 440 (473), 377 (10625), 360 (10750), 275 (48825). $\mu_{\text{eff}} = 1.78 \mu_B$ at 298 K in DMSO-*d*₆ containing 1% TMS (v/v). $\Lambda_M = 84 \text{ S m}^2 \text{ M}^{-1}$ in DMF at 25 °C.

Anal. Calc. for C₄₃H₃₄N₅O₇ClFeCu (**4**): C, 58.19; H, 3.86; N, 7.89. Found: C, 58.01; H, 4.01; N, 7.99%. Selected IR data (cm⁻¹): 3221br, 3082w, 2925w, 2327w, 2075w, 2012w, 1614vs (COO_{asym}), 1512s, 1449m, 1362s (COO_{sym}), 1236m, 1089vs (ClO₄⁻), 916w, 807s, 776s, 725s, 661w, 621s, 556w, 484s, 429m. ESI-MS in MeOH: *m/z* 787 [M-(ClO₄⁻)]⁺. UV-Vis in DMF-Tris-HCl buffer (1:4 v/v) [$\lambda_{\text{max}}/\text{nm}$ ($\epsilon/\text{M}^{-1} \text{ cm}^{-1}$)]: 615 (125), 455 (503), 301 (22225), 260 (29650). $\mu_{\text{eff}} = 1.77 \mu_B$ at 298 K in DMSO-*d*₆ containing 1% TMS (v/v). $\Lambda_M = 79 \text{ S m}^2 \text{ M}^{-1}$ in DMF at 25 °C.

2.2.2. Preparation of Fc-PheH

L-Phenylalanine (0.36 g, 1.0 mmol) was dissolved in dry methanol (10 mL) by addition of one equivalent NaOH (0.04 g, 1.0 mmol) with continuous stirring. This solution is added drop-wise to a methanol solution of ferrocenecarboxaldehyde (0.21 g, 1 mmol). The mixture was refluxed for 2 h, cooled in an ice bath and treated with 5 eq. of NaBH₄ for another ~30 min with continuous stirring. Removal of solvent resulted in a sticky mass which was dissolved in water and pH was maintained to 5–6 with dilute HCl. A brown precipitate thus appeared was isolated and thoroughly washed with water, methanol and diethyl ether and finally dried in vacuum over P₄O₁₀. Yield: 0.31 g (~85%).

Anal. Calc. for C₂₀H₂₁N₂O₂Fe (Fc-PheH): C, 66.13; H, 5.83; N, 3.86. Found: C, 66.02; H, 5.89; N, 3.79%. ESI-MS in MeOH: *m/z* 386 [M+Na⁺]. Selected IR data (cm⁻¹): 1583vs (COO_{asym}), 1495m, 1405vs (COO_{sym}), 1106w, 1028w, 998m, 856s, 746w, 699m, 551w, 478s, 444w, 415m. ¹H NMR (D₂O, ppm): δ H^{ph} (7.17, m, 5H), H^{cpo} (4.10, s, 2H), H^{cpm} (4.05, s, 2H) H^{cp} (4.02, s, 5H), H^a (3.32, d, 1H, ²J_{HH} = 12.8 Hz), H^{a'} (3.17, d, 1H, ²J_{HH} = 12.4 Hz), H^b (3.24, m, 1H), H^c (2.77, m, 2H) (vide [Supplementary data for hydrogen atom labelling](#)).

2.2.3. Preparation of [Cu(Fc-Phe)(phen)](ClO₄) (**5**)

Complex **5** was prepared by following the same procedure as described for complexes **1–4**. Yield: 0.56 g (~79%).

Anal. Calc. for C₃₂H₁₈N₃O₆ClFeCu (**5**): C, 54.48; H, 4.00; N, 5.96. Found: C, 54.19; H, 3.81; N, 6.03%. Selected IR data (cm⁻¹): 3245br, 3080w, 2937w, 2320w, 2038w, 1980w, 1630vs (COO_{asym}), 1521s, 1495w, 1430s, 1368s (COO_{sym}), 1236w, 1205w, 1097vs (ClO₄⁻), 1001m, 917m, 845s, 746m, 719s, 653w, 621s, 563m, 481s. ESI-MS in MeOH: *m/z* 605 [M-(ClO₄⁻)]⁺. UV-Vis in DMF-Tris-HCl buffer (1:4 v/v) [$\lambda_{\text{max}}/\text{nm}$ ($\epsilon/\text{M}^{-1} \text{ cm}^{-1}$)]: 605 (125), 440 (315), 273 (24360). $\mu_{\text{eff}} = 1.79 \mu_B$ at 298 K in DMSO-*d*₆ containing 1% TMS (v/v). $\Lambda_M = 82 \text{ S m}^2 \text{ M}^{-1}$ in DMF at 25 °C.

2.2.4. Preparation of Ph-TyrH and Ph-PheH

L-Tyrosine or L-phenylalanine (0.36 g of L-tyrosine or 0.33 g of L-phenylalanine, 2.0 mmol) was dissolved in dry methanol (15 mL) by addition of one equivalent of NaOH (0.08 g, 2.0 mmol) with continuous stirring. Benzaldehyde (0.2 mL, 2.0 mmol) was added drop-wise to the above solution. The mixture was refluxed for an hour, cooled and then treated with an excess of solid NaBH₄ in an ice-bath with constant stirring. After stirring for ~15–20 min the solvent was removed to get a mass which was dissolved in water and treated with dilute HCl to maintain a pH of ~5–6. A white solid precipitated out was isolated, thoroughly washed with water and cold methanol and finally dried in vacuum over P₂O₅. Yield: 0.43 g (~78%) for Ph-TyrH and 0.41 g (~80%) for Ph-PheH.

Anal. Calc. for C₁₆H₁₇NO₃ (Ph-TyrH): C, 70.83; H, 6.32; N, 5.16. Found: C, 70.55; H, 6.60; N, 5.30%. ESI-MS in MeOH: *m/z* 294 [M+Na⁺]. Selected IR data (cm⁻¹): 1580vs (COO_{asym}), 1511s, 1437m, 1390vs (COO_{sym}), 1332m, 1250s, 1104m, 1058w, 1032w, 995w, 964w, 920w, 820s, 777m, 746s, 695s, 634m, 568m, 535s, 487s. ¹H NMR (D₂O, ppm): δ H^{ph} (7.22, m, 5H), H^a (3.61, d, 1H, ²J_{HH} = 12 Hz), H^{a'} (3.43, d, 1H, ²J_{HH} = 12 Hz), H^b (3.15, m, 1H), H^c (2.65, m, 2H), H^d (6.86, d, 2H, ²J_{HH} = 8 Hz), H^e (6.52, d, 2H, ²J_{HH} = 8 Hz) (vide [Supplementary data for hydrogen atom labelling](#)).

Anal. Calc. for C₁₆H₁₇NO₂ (Ph-PheH): C, 75.27; H, 6.71; N, 5.49. Found: C, 75.09; H, 6.82; N, 5.41%. ESI-MS in MeOH: *m/z* 256 [M+H⁺], 278 [M+Na⁺]. Selected IR data (cm⁻¹): 1593vs (COO_{asym}), 1495m, 1433s, 1385vs (COO_{sym}), 1330m, 1204m, 1082m, 1029m, 971w, 916w, 865m, 804w, 745s, 694vs, 616w, 582m, 529s, 483s, 432w. ¹H NMR (D₂O, ppm): δ H^{ph,Ph'} (7.18, m, 10H), H^a (3.60, d, 1H, ²J_{HH} = 12.4 Hz), H^{a'} (3.42, d, 1H, ²J_{HH} = 12.8 Hz), H^b (3.19, m, 1H), H^c (2.75, m, 2H) (vide [Supplementary data for hydrogen atom labelling](#)).

2.2.5. Preparation of [Cu(Ph-Tyr)(L)](ClO₄) (L = phen, **6**; dppz, **7**)

Complexes **6** and **7** were prepared following a similar procedure as described for complexes **1–4**. The dark blue methanolic solution of the complex on slow evaporation gave a dark blue solid which was washed with small portions of cold methanol, water and finally dried in vacuo over P₄O₁₀ (Yield: 0.43 g, ~70% for **6**, 0.52 g, ~73% for **7**).

Anal. Calc. for C₂₈H₂₄N₃O₇ClCu (**6**): C, 54.82; H, 3.94; N, 6.85. Found: C, 54.64; H, 3.69; N, 6.99%. Selected IR data (cm⁻¹): 3120br, 3010w, 2927w, 2335w, 1637vs (COO_{asym}), 1515s, 1430s, 1378m (COO_{sym}), 1348m, 1273m, 1228m, 1090–1052vs (ClO₄⁻), 970s, 872w, 835s, 760s, 712s, 619s, 583m, 546w, 511w, 453w, 430w. ESI-MS in MeOH: *m/z* 513 [M-(ClO₄⁻)]⁺. UV-Vis in DMF-Tris-HCl buffer (1:4 v/v) [$\lambda_{\text{max}}/\text{nm}$ ($\epsilon/\text{M}^{-1} \text{ cm}^{-1}$)]: 610 (85), 272 (24475), 295sh (9000). $\mu_{\text{eff}} = 1.77 \mu_B$ at 298 K in DMSO-*d*₆ containing 1% TMS (v/v). $\Lambda_M = 66 \text{ S m}^2 \text{ M}^{-1}$ in DMF at 25 °C.

Anal. Calc. for C₃₄H₂₆N₅O₇ClCu (**7**): C, 57.07; H, 3.66; N, 9.79. Found: C, 56.91; H, 3.68; N, 10.06%. Selected IR data (KBr phase, cm⁻¹): 3225br, 3085w, 2997w, 2357w, 1643vs (COO_{asym}), 1497s, 1420m, 1357vs (COO_{sym}), 1232w, 1093–1055vs (ClO₄⁻), 923w, 817m, 762s, 728s, 620s, 577w, 425s. ESI-MS in MeOH: *m/z* 615 [M-(ClO₄⁻)]⁺. UV-Vis in DMF-Tris-HCl buffer (1:4 v/v) [$\lambda_{\text{max}}/\text{nm}$ ($\epsilon/\text{M}^{-1} \text{ cm}^{-1}$)]: 580 (124), 377 (12425), 360 (12725), 275 (52715). $\mu_{\text{eff}} = 1.80 \mu_B$ at 298 K in DMSO-*d*₆ containing 1% TMS (v/v). $\Lambda_M = 68 \text{ S m}^2 \text{ M}^{-1}$ in DMF at 25 °C.

2.2.6. Preparation of [Cu(Ph-Phe)(phen)](ClO₄) (**8**)

Complex **8** was prepared in good yield by the same procedure as described for **6** and **7**. Yield: 0.45 g (~75%).

Anal. Calc. for C₂₈H₂₄N₃O₆ClCu (**8**): C, 56.28; H, 4.05; N, 7.03. Found: C, 55.99; H, 4.01; N, 7.22%. Selected IR data (cm⁻¹): 3070br, 2933w, 2357w, 2179w, 1978w, 1610vs (COO_{asym}),

1521s, 1495m, 1440s, 1382s, 1384s (COO_{sym}), 1219w, 1093–1051vs (ClO₄⁻), 967w, 926m, 849s, 754s, 718s, 699s, 617s, 553m, 494m, 427m. ESI-MS in MeOH: *m/z* 497 [M–(ClO₄⁻)⁺]. UV–Vis in DMF–Tris–HCl buffer (1:4 v/v) [λ_{\max}/nm ($\epsilon/M^{-1}\text{cm}^{-1}$): 615 (130), 275 (41875)]. $\mu_{\text{eff}} = 1.80 \mu_{\text{B}}$ at 298 K in DMSO-*d*₆ containing 1% TMS (v/v). $\Lambda_{\text{M}} = 65 \text{ S m}^2 \text{ M}^{-1}$ in DMF at 25 °C.

2.3. Solubility and stability

The complexes were soluble in MeOH, DMF, DMSO, MeCN and in the aqueous mixtures of these solvents; less soluble in CHCl₃ and CH₂Cl₂, and insoluble in hydrocarbon solvents. They were stable in both solid and solution phases.

2.4. X-ray crystallographic procedures

The crystal structures of [Cu(Fc-Phe)(phen)](PF₆) (**5a**) and [Cu(Ph-Tyr)(phen)](ClO₄) (**6**) were obtained by single crystal X-ray diffraction method. Crystals of **5a** were obtained by slow evaporation of an aqueous methanol solution of **5** in the presence of NH₄PF₆. Crystals of **6** were obtained from the methanol solution of the complex on slow evaporation of the solvent. Crystal mounting was done on glass fibres with epoxy cement. All geometric and intensity data were collected at room temperature using an automated Bruker SMART APEX CCD diffractometer equipped with a fine focus 1.75 kW sealed tube Mo K α X-ray source ($\lambda = 0.71073 \text{ \AA}$) with increasing ω (width of 0.3° per frame) at a scan speed of 5 s per frame. Intensity data, collected using an ω -2 θ scan mode, were corrected for Lorentz-polarization effects and for absorption [62]. The structure solution was done by the combination of Patterson and Fourier techniques and refined by full-matrix least-squares method using SHELX system of programs [63]. All hydrogen atoms belonging to the complex were in their calculated positions and refined using a riding model. All non-hydrogen atoms were refined anisotropically. The perspective views of the

molecules were obtained by ORTEP [64,65]. Selected crystallographic data are given in Table 1.

2.5. DNA binding and cleavage experiments

The DNA binding and cleavage experiments were carried out using calf thymus DNA and supercoiled (SC) pUC19 DNA by following reported standard procedures [66]. For UV–Vis absorption titration, Tris–HCl buffer of pH 7.2 was used and the concentration of ct-DNA was 235 μM . DNA thermal denaturation experiments were carried out in phosphate buffer (pH 6.8) using ct-DNA of 200 μM and complexes of 20 μM by varying the temperature from 40 to 90 °C. The ratio of the complex and DNA concentration was 1:10. The DNA viscometric titrations were done in Tris–HCl buffer (pH 7.2) using ct-DNA of 160 μM . The SC pUC19 DNA cleavage activity of the complexes **1–6** was studied in visible light of 454, 568 and 647 nm wavelengths using a Spectra Physics Water-Cooled Mixed-Gas Ion Laser Stabilite® 2018-RM (continuous-wave (CW) beam diameter at $1/e^2 = 1.8 \text{ mm} \pm 10\%$ and beam divergence with full angle = 0.7 mrad $\pm 10\%$) and in the dark using external additives like glutathione (GSH) and hydrogen peroxide. Various singlet oxygen quenchers and radical scavengers were used for chemical nuclease and DNA photocleavage mechanistic studies to detect the formation of any reactive oxygen species (ROS).

2.6. Cell culture

HeLa (human cervical carcinoma) and MCF-7 (human breast adenocarcinoma) cells were maintained in Dulbecco's Modified Eagle's Medium (DMEM), supplemented with 10% foetal bovine serum (FBS), 100 IU ml⁻¹ of penicillin, 100 $\mu\text{g ml}^{-1}$ of streptomycin and 2 mM Glutamax at 37 °C in a humidified incubator at 5% CO₂. The adherent cultures were grown as monolayer and were passaged once in 4–5 days by trypsinizing with 0.25% Trypsin–EDTA.

2.7. Cell viability assay

HeLa and MCF-7 cells after treatment were subjected to MTT assay. The photocytotoxicity of the complexes was based on the ability of mitochondrial dehydrogenases in the viable cells to cleave the tetrazolium rings of MTT to form dark blue membrane impermeable crystals of formazan that were measured at 540 nm giving an estimate of the number of viable cells [67]. Approximately, 15×10^3 cells of HeLa or 2×10^4 cells of MCF-7 were plated in a 96-well culture plate in DMEM supplemented with 10% foetal bovine serum (10% DMEM) and cultured overnight. Different concentrations of the complexes were added to the cells, and incubation was continued for 4 h in the dark. After incubation, the medium was replaced with 50 mM phosphate buffer, pH 7.4 containing 150 mM NaCl (PBS) and photo-irradiation was done for 1 h in visible light of 400–700 nm using Luzchem Photoreactor (Model LZC-1, Ontario, Canada; light fluence rate: 2.4 mW cm⁻²; light dose = 10 J cm⁻²). PBS was replaced with 10% DMEM after irradiation. Incubation was continued for a further period of 20 h in dark followed by addition of 25 μL of 4 mg ml⁻¹ of MTT to each well and incubated for an additional 3 h. The culture medium was discarded, and a 200 μL volume of DMSO was added to dissolve the formazan crystals. The absorbance at 540 nm was determined using an ELISA microplate reader (BioRad, Hercules, CA, USA). The cytotoxicity of the test compounds was measured as the percentage ratio of the absorbance of the treated cells over the untreated controls. The IC₅₀ values were determined by nonlinear regression analysis (GraphPad Prism).

Table 1
Selected crystallographic data for the complexes [Cu(Fc-Phe)(phen)](PF₆) (**5a**) and [Cu(Ph-Tyr)(phen)](ClO₄) (**6**).

	[Cu(Fc-Phe)(phen)](PF ₆)	[Cu(Ph-Tyr)(phen)](ClO ₄)
Empirical formula	C ₃₂ H ₂₈ CuF ₆ FeN ₃ O ₂ P	C ₃₀ H ₂₄ ClCuN ₃ O ₇
Formula weight (g M ⁻¹)	750.93	613.49
Crystal system	Monoclinic	Triclinic
Space group	C2	P1
<i>Unit cell dimensions</i>		
<i>a</i> (Å)	20.5815(13)	7.9670(5)
<i>b</i> (Å)	11.0487(5)	9.0097(6)
<i>c</i> (Å)	15.7115(9)	9.5968(6)
α (°)	90.00	82.528(2)
β (°)	121.622(5)	77.484(2)
γ (°)	90.00	78.595(3)
<i>V</i> (Å ³)	3042.3(3)	656.47(7)
<i>Z</i>	4	1
<i>T</i> (K)	293(2)	296(2)
ρ_{calc} (g cm ⁻³)	1.639	1.552
λ (Å) (Mo K α)	0.71073	0.71073
μ (cm ⁻¹)	1.301	0.987
Data/restraints/parameters	5298/ 1/ 415	4085/ 3/ 363
<i>R</i> (000)	1524	315
Goodness-of-fit (GOF) on <i>F</i> ²	0.970	1.026
<i>R</i> (<i>F</i> _o) ^a , 1 > 2 σ (1) [<i>wR</i> (<i>F</i> _o) ^b]	0.0404 [0.0980]	0.0317 [0.0858]
<i>R</i> (all data) [<i>wR</i> (all data)]	0.0531 [0.1031]	0.0331 [0.0867]
Largest diff. peak and hole (e Å ⁻³)	0.406, -0.355	0.591, -0.329

^a $R = \sum ||F_o| - |F_c|| / \sum |F_o|$.

^b $wR = \{ \sum [w(F_o^2 - F_c^2)]^2 / \sum [w(F_o^2)]^2 \}^{1/2}$; $w = [\sigma^2(F_o) + (AP)^2 + BP]^{-1}$, where $P = (F_o^2 + 2F_c^2)/3$, $A = 0.0519$; $B = 0.0000$ for **5a** and $A = 0.0626$; $B = 0.0489$ for **6**.

2.8. Nuclear staining experiment

HeLa cells cultured on cover slips were photo-irradiated with visible light of 400–700 nm (light fluence rate = 2.4 mW cm⁻²; light dose = 10 J cm⁻²) following 4 h of incubation in the dark in the presence of 5 μM of complex **3**. The cells were then allowed to recover for 2 h, washed three times with PBS and stained with acridine orange/ethidium bromide (AO/EB) mixture (1:1, 10 μM) for 15 min and observed at 20× magnification with a fluorescence microscope (Carl Zeiss). The images were analyzed using the “Image J” image browser [68].

2.9. Fluorescence microscopy

HeLa cells (4 × 10⁴ cells/mm²), plated on cover slips, were incubated with 5 μM of the nip complex **4** for different time intervals from 1 to 4 h in dark, fixed with 4% paraformaldehyde for 10 min at room temperature and washed with PBS. This was followed by incubation with PI staining solution (50 μg/ml RNase A, 20 μg/ml PI in PBS) for 1 h at 42 °C. The cells were washed free of excess PI and mounted in 90% glycerol solution containing Mowiol, an anti-fade reagent, and sealed. Images were acquired using Apo-tome.2 fluorescence microscope (Carl Zeiss, Germany) using an oil immersion lens at 63× magnification. The images were analyzed using the AxioVision Rel 4.8.2 (Carl Zeiss, Germany) software [69].

3. Results and discussion

3.1. Synthesis and general aspects

Copper(II) complexes [Cu(Fc-Tyr)(L)](ClO₄) (**1–4**) having ferrocene-conjugated *l*-tyrosine reduced Schiff base and *N,N*-donor heterocyclic bases (L: phen, **1**; dpq, **2**; dppz, **3**; nip, **4**) were prepared in good yield from the reaction of ferrocenylmethyltyrosine (Fc-TyrH) with copper(II) acetate monohydrate and the respective phenanthroline base in methanol. Complex of ferrocenylmethylphenylalanine and 1,10-phenanthroline, viz., [Cu(Fc-Phe)(phen)](ClO₄) (**5**) was prepared by reacting the ligands with copper(II) acetate monohydrate and structurally characterized by X-ray crystallography. To explore the effect of the ferrocenyl moiety on the overall DNA cleavage activity and photocytotoxicity of **1–5**, three control complexes, viz., [Cu(Ph-Tyr)(L)](ClO₄) with L as phen (in **6**) and dppz (in **7**), where Ph-TyrH is the reduced Schiff base derived from benzaldehyde and *l*-tyrosine and [Cu(Ph-phe)(phen)](ClO₄) (**8**), where Ph-Phe is the reduced Schiff base of benzaldehyde and *l*-phenylalanine were prepared. The complexes were characterized

by various spectroscopic and analytical methods. Selected physico-chemical data are given in Table 2. The complexes are stable in a solution phase as evidenced from their ESI-MS spectra showing essentially the molecular ion peak as [M-(ClO₄)]⁺ in methanol. Complexes **6–8** show mass spectral peaks that correspond to the species showing loss of perchlorate ligand in methanol, while the complexes have a metal-bound perchlorate ligand in the solid state. The IR spectra of the complexes display characteristic stretching bands at ~1630 cm⁻¹ and ~1360 cm⁻¹ due to COO of the amino acid. The complexes also show characteristic stretching bands for ClO₄⁻ at ~1080 cm⁻¹. There is, however, broadening and splitting of the ClO₄⁻ band observed in the IR spectra of complexes **6–8** indicating the presence of metal bound ClO₄⁻ ligand [70,71]. The IR spectral data reveal the structural differences of the two types of complexes having or not having the ferrocenyl moiety. The complexes **1–5** are 1:1 electrolytic in nature with molar conductance value of ~80 S m² M⁻¹ in DMF at 25 °C [72]. Complexes **6–8** are also 1:1 electrolytic with the loss of the coordinated ClO₄⁻ in the solution state giving molar conductance value of ~65 S m² M⁻¹ in DMF at 25 °C. Magnetic moment values of ~1.8 μ_B at 25 °C suggest the presence of a one-electron paramagnetic 3d⁹-Cu(II) center in all the complexes. The UV-Vis spectra of **1–8**, recorded in DMF-Tris-HCl buffer (1:4 v/v), display a broad and weak copper-centered d-d band in the range of 580–615 nm (Fig. 2). A moderately intense ferrocene-centered band is observed near 440 nm in **1–5** [73]. The ligand-centered electronic transitions are observed in the UV region. Complex **4** exhibits an emission spectral band at 418 nm on excitation at 300 nm in DMF at 25 °C with a quantum yield (φ) value of 0.11 (Fig. 2). The emissive property of this complex is used for cellular imaging. Complexes **1–5** show quasi-reversible cyclic voltammetric response at ~0.5 V vs. SCE in DMF-0.1 M TBAP due to the Fc⁺-Fc couple (Table 2). There is a significant positive shift of ~100 mV of the Fe(III)-Fe(II) potential in **1–5** compared to that of ferrocene (0.43 V). The complexes also show a quasi-reversible cyclic voltammetric response near -0.1 V due to the Cu(II)-Cu(I) couple. Complexes **6–8** show the Cu(II)-Cu(I) quasi-reversible response near -0.12 V vs. SCE. The ligand reduction peaks appear near -1.1 and -1.7 V. The minor difference in the Cu(II)/Cu(I) redox values observed between two different types of complexes is probably due their structural similarities in the solution phase.

3.2. Crystal structure

Complex **5** as its hexafluorophosphate salt (**5a**) and complex **6** were structurally characterized by single crystal X-ray diffraction method. Complex **5a** crystallized in the C2 space group of the

Table 2

Selected physicochemical data for the complexes [Cu(Fc-Tyr)(L)](ClO₄) (L = phen, **1**; dpq, **2**; dppz, **3**; nip, **4**), [Cu(Fc-Phe)(phen)](ClO₄) (**5**), [Cu(Ph-Tyr)(L)](ClO₄) (L = phen, **6**; dppz, **7**) and [Cu(Ph-Phe)(phen)](ClO₄) (**8**).

Complex	IR/cm ⁻¹ [ν(ClO ₄ ⁻)]	λ _{max} /nm (ε/M ⁻¹ cm ⁻¹) ^a	E _f /V (ΔE _p /mV) ^b		Λ _m ^c /S m ² M ⁻¹	μ _{eff} ^d /μ _B
			Fc ⁺ -Fc	Cu(II)-Cu(I)		
1	1096	440 (297), 590 (119)	0.49 (98)	-0.13 (410)	79	1.80
2	1086	452 (298), 595 (123)	0.49 (95)	-0.12 (470)	82	1.81
3	1075	440 (473), 585 (129)	0.50(80)	-0.11 (490)	84	1.78
4	1089	455 (503), 615 (125)	0.50 (110)	-0.16 (400)	80	1.79
5	1097	440 (315), 605 (125)	0.49 (110)	-0.15 (300)	82	1.79
6	1071	610 (85)	-	-0.14 (380)	66	1.77
7	1074	580 (124)	-	-0.12 (457)	68	1.80
8	1072	615 (130)	-	-0.13 (270)	65	1.80

^a In DMF-Tris-HCl buffer (1:4 v/v). The bands at ~450 and 600 nm are ferrocene-based and Cu(II)-based, respectively.

^b Fc⁺-Fc and Cu(II)-Cu(I) couple in DMF-0.1 M TBAP, E_f = 0.5(E_{pa} + E_{pc}), ΔE_p = (E_{pa} - E_{pc}), where E_{pa} and E_{pc} are the anodic and cathodic peak potentials, respectively. The potentials are vs. SCE. Scan rate = 50 mV s⁻¹.

^c Molar conductivity in DMF.

^d Magnetic moment at 298 K using DMSO-d₆ solution of the complexes.

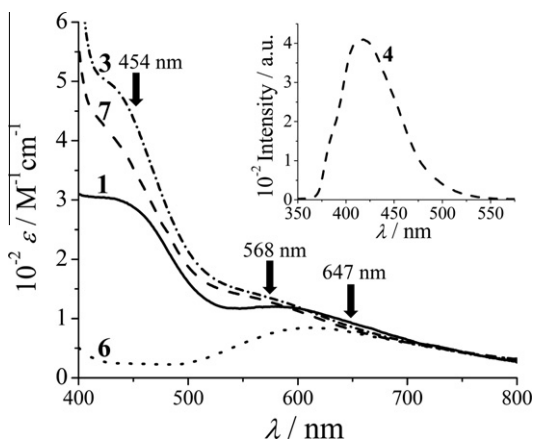


Fig. 2. The electronic spectra of $[\text{Cu}(\text{Fc-Tyr})(\text{L})](\text{ClO}_4)$ [$\text{L} = \text{phen}$ in **1** (—); dppz in **3** (---)] and $[\text{Cu}(\text{Ph-Tyr})(\text{L})](\text{ClO}_4)$ [$\text{L} = \text{phen}$ in **6** (···); dppz in **7** (---)] in DMF–Tris–HCl buffer (1:4 v/v). The arrows indicate the wavelengths of light used for the photo-induced DNA cleavage studies. The inset shows the emission spectrum of $[\text{Cu}(\text{Fc-Tyr})(\text{nip})](\text{ClO}_4)$ (**4**, ···) in DMF.

monoclinic crystal system with four molecules in the unit cell. Complex **6** crystallized in the $P1$ space group of the triclinic crystal system with one molecule in the unit cell. The ORTEP views of the complexes are shown in Figs. 3 and 4. Selected bond distances and angles data are given in Table 3. Complex **5a** is a heterobimetallic species having the Cu(II) and Fe(II) centers. The X-ray structure shows a square-planar geometry of Cu(II) in a CuN_3O coordination environment ($\tau = 0.071$) [74]. This geometry is favored due to the steric requirements of the reduced Schiff base ligand where both sides of the square plane are blocked by the phenyl and ferrocenyl groups. Both the Fc-Phe and phenanthroline ligands coordinate in a bidentate fashion. The Cu–N and Cu–O bond distances are 2.009(4) and 1.923(3) Å, respectively, for the Fc-Phe ligand. The Cu–N bond distances are 1.987(4) and 2.007(4) Å for the heterocyclic base. The cyclopentadienyl (Cp) rings of the ferrocenyl moiety are in a nearly eclipsed conformation with a dihedral angle between the $\eta^5\text{-C}_5\text{H}_5$ and $\eta^5\text{-C}_5\text{H}_4$ rings of 2.38° . The average Fe–C distance is 2.038 Å. The chiral carbon of L-phenylalanine in Fc-Phe ligand retains its “S”-configuration.

The structure of **6** consists of a discrete complex having Cu(II) as the metal center. The metal exhibits an axially elongated distorted square-pyramidal CuN_3O_2 geometry ($\tau = 0.125$) with the perchlorate ion occupying the elongated fifth coordination site. The equatorial and axial Cu–O bond distances are 1.958(3) and 2.555(4) Å,

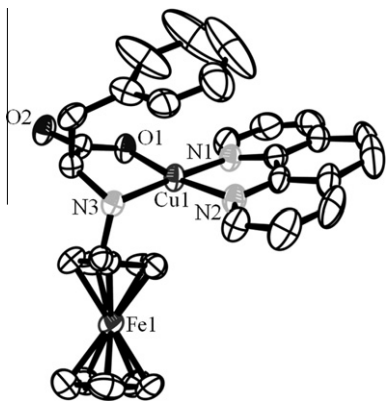


Fig. 3. ORTEP view of the cationic complex in $[\text{Cu}(\text{Fc-Phe})(\text{phen})](\text{PF}_6)$ (**5a**) showing 50% probability thermal ellipsoids and the atom numbering scheme for the metal and hetero atoms.

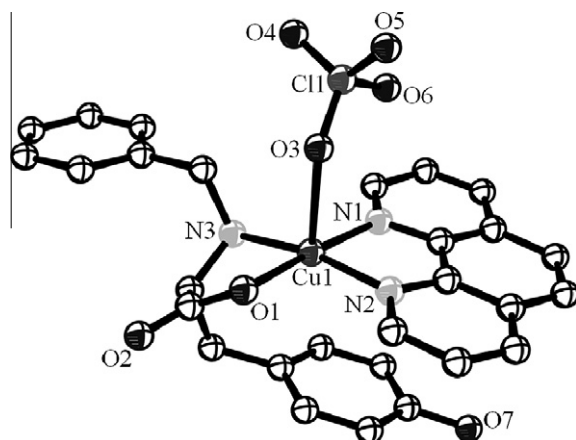


Fig. 4. ORTEP view of $[\text{Cu}(\text{Ph-Tyr})(\text{phen})](\text{ClO}_4)$ (**6**) showing 50% probability thermal ellipsoids and the atom numbering scheme for the metal and hetero atoms.

Table 3

Selected bond distances (Å) and bond angles ($^\circ$) of $[\text{Cu}(\text{Fc-Phe})(\text{phen})](\text{PF}_6)$ (**5a**) and $[\text{Cu}(\text{Ph-Tyr})(\text{phen})](\text{ClO}_4)$ (**6**).

	$[\text{Cu}(\text{Fc-Phe})(\text{phen})](\text{PF}_6)$ (5a)	$[\text{Cu}(\text{Ph-Tyr})(\text{phen})](\text{ClO}_4)$ (6)
Cu1–O1	1.923(3)	1.958(3)
Cu1–N1	1.987(4)	1.968(3)
Cu1–N2	2.007(4)	1.986(3)
Cu1–N3	2.009(4)	2.022(3)
O1–Cu1–N1	92.82(16)	176.08(15)
O1–Cu1–N2	170.94(17)	93.11(13)
N1–Cu1–N2	81.93(15)	83.10(14)
O1–Cu1–N3	85.71(12)	83.25(12)
N1–Cu1–N3	175.23(17)	100.28(12)
N2–Cu1–N3	100.10(17)	168.56(12)
Fe(1)–C ₀ ¹	1.648 ^a	–
Fe(1)–C ₀ ²	1.655 ^a	–

^a C₀¹ and C₀² are two centroids of the Cp rings in the ferrocenyl moiety comprising of atoms C(23) to C(27) and C(28) to C(32), respectively.

respectively. The Ph-Tyr ligand shows bidentate N,O -coordination to the Cu(II) center. The phenanthroline base coordinates in a bidentate fashion with two Cu–N bond distances within 1.968(3) to 2.022(3) Å. The chiral carbon of L-tyrosine has an “S”-configuration. The IR and X-ray crystal structural data show major structural differences for the ferrocenyl-conjugates from their non-ferrocenyl analogues in the solid state.

3.3. DNA binding properties

The affinity of the complexes to bind to calf-thymus DNA was studied using spectral, DNA melting and viscometric methods. Selected DNA binding data are presented in Table 4. UV–Vis absorption titration method was used to determine the intrinsic DNA binding constant (K_b) of the complexes by monitoring the change in the absorption intensity of the ligand-centered band of the complexes **1–8** at ~ 270 nm. Significant hypochromicity with minor bathochromic shift suggests primarily groove binding nature of the complexes to ct-DNA in Tris–HCl buffer medium. Classical DNA intercalators that π -stack between two DNA base pairs are known to cause much larger hypochromicity with bathochromic shift of the spectral bands [75]. The K_b values of the complexes range within $(5.0 \pm 0.2) \times 10^4$ to $(4.2 \pm 0.4) \times 10^5 \text{ M}^{-1}$ giving the DNA binding affinity order as: **3** \approx **7** > **4** \approx **2** > **1** \approx **5** > **6** \approx **8** [76,77]. Complex **3** having an extended aromatic phenazine ring shows highest ct-DNA binding strength compared to its dpq and

phen analogues. The phenanthroline complexes **1**, **5** and **8** showed similar DNA binding propensities.

The DNA melting temperature which gives a measure of the duplex stability can be used to study the binding interactions of the complexes to DNA. The DNA duplex on melting unwinds to give single stranded DNA resulting in an increase in the absorbance at 260 nm as the bases separate out from each other. An increase in the DNA melting temperature indicates the stability of double helix. A DNA intercalator like ethidium bromide (EB) generally increases the stability of the double helix rendering thermal denaturation more difficult [78]. A significant stabilization of the ct-DNA was observed on treatment with complex **3** compared to the untreated sample giving a ΔT_m value of 4.5 °C. The ΔT_m values range within 1.0–4.5 °C for **1–8** with EB giving a ΔT_m value of 11.2 °C indicating primarily groove binding nature of the complexes with partial intercalation for complex **3** (Fig. 5a).

Viscometric titration experiments were performed to investigate the change in the relative specific viscosity of the ct-DNA on interacting with the complexes. It is known that an increase in the contour length of DNA results in an increase in its relative viscosity. Classical intercalator like EB is known to show significant increase in the relative viscosity of the DNA solution [79]. In contrast, groove binding or partially intercalating molecules cause little or no effect on the relative viscosity of the DNA solution. Hoechst dye, which is a DNA groove binder, shows only minor change in the viscosity of ct-DNA. The plots of relative viscosity $(\eta/\eta_0)^{1/3}$ vs. [complex]/[DNA] ratio, where η and η_0 are the specific viscosity of DNA in the presence and absence of the complex, respectively, for **1–5**, ethidium bromide and Hoechst dye indicate primarily surface aggregation and/or groove binding nature of the complexes (Fig. 5b). Complex **3** with an extended phenazine ring in the dppz ligand shows significant increase in the ct-DNA viscosity.

3.4. DNA cleavage study

3.4.1. Chemical nuclease activity

The chemical nuclease activity of the complexes **1–8** (10 μ M) was studied in the presence of external reagents, viz., glutathione (GSH, 1 mM) as a reducing agent and hydrogen peroxide (H_2O_2 , 200 μ M) as an oxidizing agent using SC pUC19 DNA (0.2 μ g, 30 μ M) in 50 mM Tris–HCl/50 mM NaCl buffer of pH 7.2 (Fig. 6). GSH and H_2O_2 were chosen because of the presence of Fe(III)–Fe(II) and Cu(II)–Cu(I) redox couples in the complexes **1–5**. Complexes **1–5** showed significant chemical nuclease activity in the presence of both H_2O_2 and GSH. Complexes **1** and **3** showed moderately higher chemical nuclease activity in the presence of the oxidizing agent compared to their non-ferrocenyl analogues **6** and **7** due to the involvement of the redox active ferrocenyl moiety. Control experiments with the ligands, the copper(II) salt, H_2O_2 or GSH alone did not show any significant cleavage of SC DNA under similar experimental conditions. Although ferrocenylated lysine conjugate is reported to cleave DNA in the presence of reducing agents at high complex concentration, Fc-TyrH or Fc-PheH did

not show any significant chemical nuclease activity in the concentration range used for our experiments [80]. The chemical nuclease activity follows the order: **3** (Fc-Tyr-dppz) \approx **7** (Ph-Tyr-dppz) $>$ **2** (Fc-Tyr-dpq) \approx **4** (Fc-Tyr-nip) $>$ **1** (Fc-Tyr-phen) \approx **5** (Fc-Phe-phen) $>$ **6** (Ph-Tyr-phen) \approx **8** (Ph-Phe-phen). The nuclease activity is found to generally correlate with the duplex DNA binding order of the complexes.

The mechanistic aspects of the chemical nuclease activity was evaluated using additives, viz., hydroxyl radical scavengers (catalase, DMSO, KI) and singlet oxygen quenchers (NaN_3 and TEMP). Addition of hydroxyl radical scavengers is found to inhibit the DNA cleavage activity of the complexes, while singlet oxygen quenchers show no apparent effect in the presence of GSH or H_2O_2 . The results indicate the involvement of hydroxyl radicals as the DNA cleaving agents. DNA major groove binder methyl green and DNA minor groove binder distamycin-A were used to study the groove binding preferences of the complexes. The chemical nuclease activity of **1** and **2** gets significantly inhibited in the presence of distamycin (100 μ M), while no apparent effect is there in the presence of methyl green (100 μ M) indicating minor groove binding preference of these complexes. Complex **3** showed inhibition in the presence of methyl green and not with distamycin suggesting its major groove binding preference.

3.4.2. DNA photocleavage activity

The ability of the complexes to cleave DNA when irradiated with visible laser radiation was studied using supercoiled (SC) pUC19 DNA (30 μ M, 0.2 μ g) in Tris–HCl/NaCl (50 mM, pH, 7.2) buffer (Figs. 7 and 8). Monochromatic visible light of wavelengths 454, 568 and 647 nm of 50 mW laser power were used from a tunable continuous-wave (CW) Ar–Kr mixed-gas ion laser to carry out the photo-induced DNA cleavage reactions. The wavelengths were chosen based on the presence of two metal-centered electronic spectral bands of the complexes near 450 and 600 nm (Fig. 2). Control experiments using DNA alone showed no apparent photocleavage of DNA in visible light. The phen complexes **1** and **5** (20 μ M) showed moderate DNA cleavage activity when irradiated with blue light of 454 nm giving \sim 50% cleavage of SC DNA to its NC form. Complexes **2–4** (20 μ M) nicked $>$ 80% of SC DNA in blue light. Control complexes **6–8** having the Ph-Tyr or Ph-Phe ligand showed much lower DNA photocleavage activity than their ferrocenyl analogues. The cleavage activity using 454 nm laser light follows the order: **3** [(Fc-Tyr)-Cu-(dppz)] $>$ **4** [(Fc-Tyr)-Cu-(nip)] \approx **2** [(Fc-Tyr)-Cu-(dpq)] $>$ **7** [(Ph-Tyr)-Cu-(dppz)] $>$ **1** [(Fc-Tyr)-Cu-(phen)] \approx **5** [(Fc-Phe)-Cu-(phen)] $>$ **6** [(Ph-Tyr)-Cu-(phen)] \approx **8** [(Ph-Phe)-Cu-(phen)] (Fig. 7).

The complexes showed significant photo-induced DNA cleavage activity in green light of 568 nm and red light of 647 nm. A 25 μ M dppz complex **3** in green light gave \sim 85% cleavage of SC DNA. The dpq complex **2** and nip complex **4** cleaved $>$ 70% of the SC DNA in green light. The phen complexes **1** and **5** (25 μ M) displayed lower DNA cleavage activity probably due to photo-inactive nature of phen. The complexes also displayed significant DNA cleavage activity in red light of 647 nm. Complexes **2–4** (25 μ M) cleaved $>$ 70% of

Table 4

DNA binding data for [Cu(Fc-Tyr)(L)](ClO₄) (L = phen, **1**; dpq, **2**; dppz, **3**; nip, **4**), [Cu(Fc-Phe)(phen)](ClO₄) (**5**), [Cu(Ph-Tyr)(L)](ClO₄) (L = phen, **6**; dppz, **7**) and [Cu(Ph-Phe)(phen)](ClO₄) (**8**).

	1	2	3	4	5	6	7	8
K_b^a/M^{-1}	$(7.6 \pm 0.5) \times 10^4$	$(2.3 \pm 0.5) \times 10^5$	$(4.2 \pm 0.4) \times 10^5$	$(2.1 \pm 0.6) \times 10^5$	$(7.4 \pm 0.3) \times 10^4$	$(5.1 \pm 0.4) \times 10^4$	$(4.0 \pm 0.3) \times 10^5$	$(5.0 \pm 0.2) \times 10^4$
S^b	0.09	0.12	0.16	0.11	0.09	0.04	0.12	0.05
$\Delta T_m^c / ^\circ C$	1.4	2.4	4.5	2.7	1.3	1.0	3.5	1.1

^a Intrinsic equilibrium DNA binding constant from the UV–Vis experiment.

^b Binding site size.

^c Change in the calf thymus DNA melting temperature.

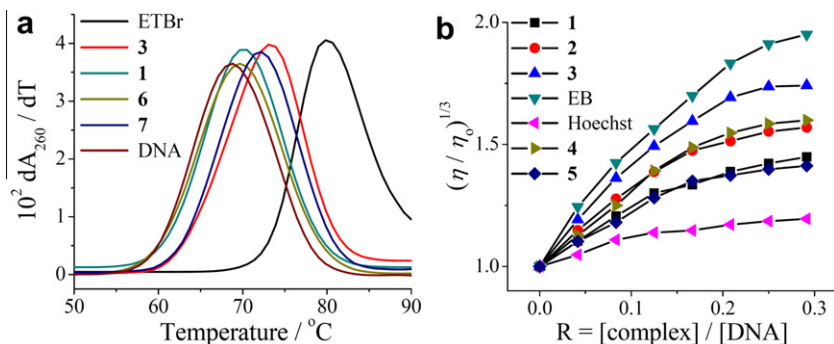


Fig. 5. (a) DNA melting temperature plot using ct-DNA (200 μ M NP) in the absence and presence of 20 μ M ethidium bromide (EB) and complexes **1**, **3**, **6** and **7** in 5 mM phosphate buffer (pH 6.8); (b) The effect of increasing concentration of EB (\blacktriangledown), Hoechst dye (\blacktriangleleft), **1** (\blacksquare), **2** (\bullet), **3** (\blacktriangle), **4** (\blacktriangleright) and **5** (\blacklozenge) on the relative viscosity of ct-DNA at 37.0(\pm 0.1) $^{\circ}$ C in 5 mM Tris-HCl buffer (pH 7.2, [ct-DNA] = 160 μ M).

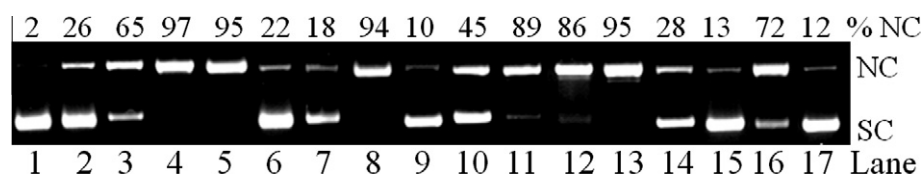


Fig. 6. Gel electrophoresis diagram showing the chemical nuclease activity of the complexes **1–8** (10 μ M) using SC pUC19 DNA (0.2 μ g, 30 μ M b.p.) in the presence of 1.0 mM glutathione (GSH) as a reducing (lanes 2–9) and 200 μ M H_2O_2 as an oxidizing agent (lanes 10–17) for an incubation time of 2 h: lane-1, DNA control; lane-2, DNA + **1**; lane-3, DNA + **2**; lane-4, DNA + **3**; lane-5, DNA + **4**; lane-6, DNA + **5**; lane-7, DNA + **6**; lane-8, DNA + **7**; lane-9, DNA + **8**; lane-10, DNA + **1**; lane-11, DNA + **2**; lane-12, DNA + **3**; lane-13, DNA + **4**; lane-14, DNA + **5**; lane-15, DNA + **6**; lane-16, DNA + **7**; lane-17, DNA + **8**.

the SC DNA in red light. The role of the ferrocenyl moiety in the DNA photo-cleavage reactions is evidenced from the greater activity of the ferrocenyl complexes **1**, **3** and **5** than their phenyl analogues **6–8**. Complexes **1** and **3** showed remarkable DNA cleavage activity in green and red light. The cleavage activity in green and red light follows a similar order as observed for blue light (Table 5). Control experiments using copper(II) perchlorate and the ligands alone did not show any significant DNA photocleavage activity under similar reaction conditions. Ferrocene derivatives like 4-ferrocenylbutanoate are known to generate radical species under high energy flash photolysis conditions due to their photo-oxidation, but the ferrocenylated amino acid ligands used in the present study did not show any apparent DNA photocleavage activity when

irradiated with low energy light within the PDT spectral window [81].

Complexes **6–8** lacking the ferrocenyl moiety showed significant DNA hydrolytic cleavage activity in dark. Complex **6** showed \sim 23% cleavage of SC DNA in dark without any external agents where as its ferrocenyl analogue showed only \sim 9% cleavage. The labile axial ClO_4^- ligand in **6–8** undergoes dissociation in aqueous buffer and the resulting species could bind the phosphodiester bond causing hydrolytic damage of DNA. In contrast, the Fc-Tyr complexes are structurally rigid due to steric protection of two axial sites. The complexes did not show any significant DNA photocleavage activity under argon suggesting possible involvement of the reactive oxygen species (ROS) in the DNA cleavage reactions.

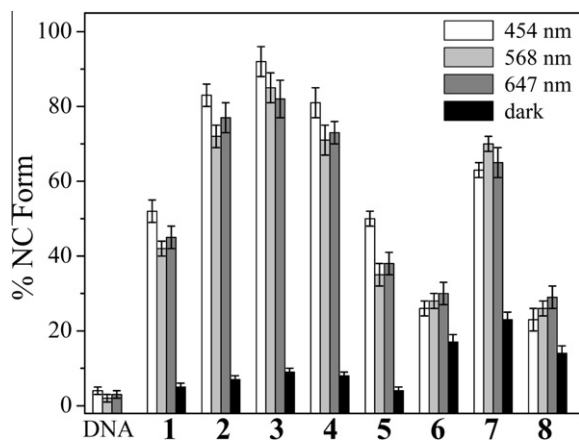


Fig. 7. Bar diagram showing visible light-induced DNA cleavage activity of the complexes **1–8** using SC pUC19 DNA (0.2 μ g, 30 μ M b.p.) for an exposure time of 2 h and laser power of 50 mW. [Complex] = 20 μ M for 454 nm and 25 μ M for other wavelengths. Colour code: white, 454 nm light; light gray, 568 nm light; dark gray, 647 nm light; black, sample unexposed to light.

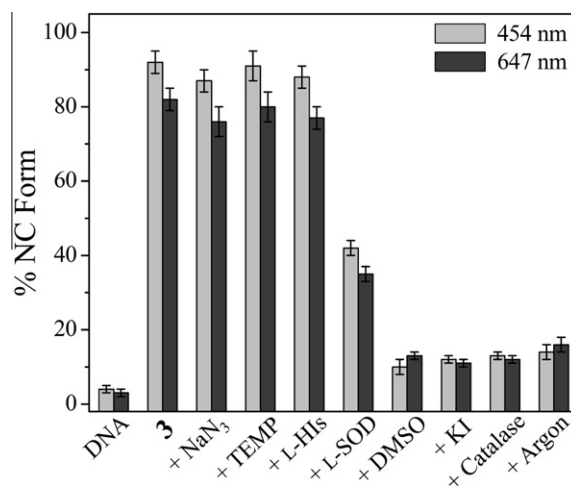


Fig. 8. Bar diagram showing the mechanistic data for the visible light-induced DNA cleavage activity of [Cu(Fc-Tyr)(dppz)](ClO_4) (**3**) at 454 nm (20 μ M) and 647 nm (25 μ M) using SC pUC19 DNA (0.2 μ g, 30 μ M b.p.) for an exposure time of 2 h. Colour code: light gray, 454 nm; black, 647 nm.

Table 5

Selected DNA (SC pUC19, 0.5 μg) cleavage data for [Cu(Fc-Tyr)(L)](ClO₄) (L = phen, **1**; dpq, **2**; dppz, **3**; nip, **4**), [Cu(Fc-Phe)(phen)](ClO₄) (**5**), [Cu(Ph-Tyr)(L)](ClO₄) (L = phen, **6**; dppz, **7**) and [Cu(Ph-Phe)(phen)](ClO₄) (**8**) in visible light.

Reaction conditions ^a	%NC form ($\lambda = 454 \text{ nm}$)	%NC form ($\lambda = 568 \text{ nm}$)	%NC form ($\lambda = 647 \text{ nm}$)
DNA control	4	2	3
DNA + 1	52	42	45
DNA + 2	82	73	77
DNA + 3	92	85	82
DNA + 4	81	71	73
DNA + 5	48	37	40
DNA + 6	26	28	30
DNA + 7	63	70	65
DNA + 8	23	26	29

^a In Tris-buffer medium (pH 7.2). λ , Laser wavelength. Photo-exposure time (t) = 2 h. Concentration of the complexes **1–6** was 20 μM for the 454 nm and 25 μM for the 568 and 647 nm experiments.

The ROS could form following either type-I and/or type-II pathway. To ascertain this, mechanistic aspects of the DNA photocleavage reactions were studied in visible light of 454 and 647 nm wavelengths using the dppz complex **3** and different additives (Fig. 8). Singlet oxygen quenchers, viz., NaN₃, TEMP or L-histidine did not show any significant inhibition in the DNA cleavage activity thus eliminating the involvement of a type-II process. The hydroxyl radical scavengers, viz., DMSO, KI and catalase showed significant inhibition in the DNA photocleavage suggesting the formation of hydroxyl radical via a photo-redox pathway [36–40]. Partial inhibition in the DNA photocleavage activity was observed on addition of superoxide dismutase (SOD) indicating formation of superoxide radical anion as an intermediate species [82].

3.5. Cytotoxicity study

Cellular toxicity of the complexes **1–6** against HeLa (human cervical carcinoma) and MCF-7 (human breast adenocarcinoma) cancer cell lines in dark and visible light was evaluated from the MTT assay (Figs. 9 and 10). A dose dependent anti-proliferative activity of the complexes was observed against both HeLa and MCF-7 cells in dark as expected due to reduction of copper(II) to copper(I) by thiols like GSH and cysteine and subsequent generation of radicals. Photo-irradiation of the samples with visible light of 400–700 nm resulted in an enhanced cytotoxicity of the complexes. The ferrocenyl complexes were found to be more photo-cytotoxic in both the cell lines compared to the non-ferrocenyl analogues probably due to the involvement of the ferrocene moiety. An enhancement in the cytotoxicity of the complexes in HeLa cells was observed when exposed to visible light compared to the samples in dark. The dppz complex **3** was most toxic to HeLa cells with an IC₅₀ value of 0.9 μM when exposed to visible light. The IC₅₀ values of the complexes along with Photofrin and cisplatin are given in Table 6 [37,83]. The observed photocytotoxicity of the complexes is comparable to that of Photofrin. Cisplatin lacking any photoactive moiety showed an IC₅₀ value of $\sim 70 \mu\text{M}$ in both dark and light under similar experimental conditions. Photo exposure of the cells in absence of the complex showed no apparent reduction in the cell viability. A similar photo-enhanced anti-proliferative behaviour of the complexes was seen on the breast cancer cell line (MCF-7) on exposure to visible light. Again, the dppz complex **3** was most cytotoxic towards MCF-7 cells giving an IC₅₀ of 0.76 μM in visible light. The activities of the complexes are similar in both the cell lines used. The ligands or the metal salt alone were significantly non-toxic both in dark and visible light. The dpq complex **2** was found

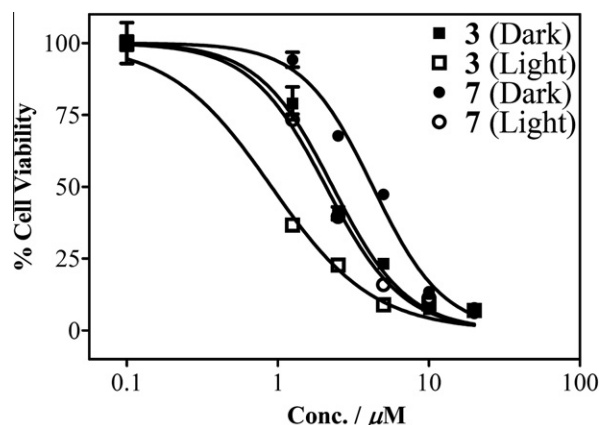


Fig. 9. Cell viability plots for the cytotoxic effect of the dppz complexes **3** (■) and **7** (●) in HeLa cells in dark (solid symbols) and in the presence of visible light (hollow symbols, 400–700 nm, 10 J cm⁻²).

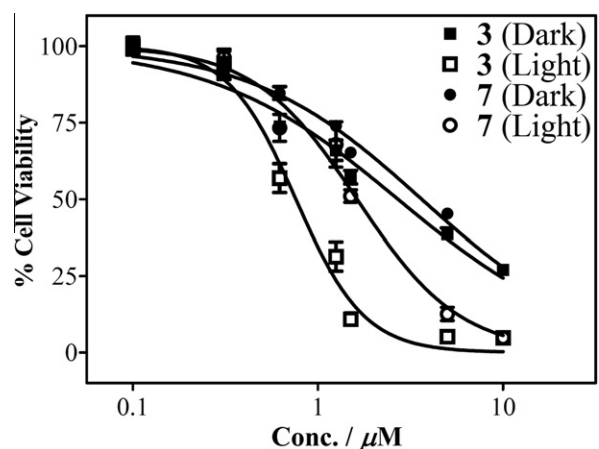


Fig. 10. Cell viability plots for the cytotoxic effect of the dppz complexes **3** (■) and **7** (●) in MCF-7 cells in dark (solid symbols) and in the presence of visible light (hollow symbols, 400–700 nm, 10 J cm⁻²).

to be relatively non-toxic compared to the other complexes and this could be due to its reduced uptake or quick efflux from the cancer cells.

3.6. Acridine orange/ethidium bromide dual staining

The mechanistic aspects of the cell death were obtained from acridine orange/ethidium bromide (AO/EB) dual staining of the HeLa cells treated with complex **3** (Fig. 11). EB being unable to enter the cells with intact cell membrane, stains only the nucleus of late apoptotic cells with intense red colour. This gives an idea of the cell death based on the changes in nuclear morphology upon PDT [37,84]. The cells treated with complex **3** in dark showed no apparent change in the nuclear morphology and no apparent EB staining. In contrast, the cells treated with 5 μM of complex **3** and photo-irradiated with visible light displayed significant increase in the apoptotic nuclear morphology wherein the nuclei had condensed significantly with intense EB staining and no AO staining (Fig. 11, panels (c) and (d)). Cells cultured in the dark and the cells with DMSO control showed negligible nuclear condensation and no EB staining (Fig. 11, panels (a) and (b)). The results indicate that the photo-irradiated cells are in the late stage of apoptosis, which enables EB to enter the cells and stain the nucleus.

Table 6
A comparison of the IC₅₀ values of [Cu(Fc-Tyr)(L)](ClO₄) (L = phen, **1**; dpq, **2**; dppz, **3**; nip, **4**), [Cu(Fc-Phe)(phen)](ClO₄) (**5**), [Cu(Ph-Tyr)(L)](ClO₄) (L = phen, **5**; dppz, **6**) and [Cu(Ph-Phe)(phen)](ClO₄) (**8**) with Photofrin[®] and cisplatin in HeLa and MCF-7 cancer cells.

Compound	HeLa		MCF-7	
	IC ₅₀ (μM) dark ^a	IC ₅₀ (μM) visible light ^b	IC ₅₀ (μM) dark ^a	IC ₅₀ (μM) visible light ^b
1	9.33 (±0.28)	4.63 (±0.15)	9.29 (±0.22)	5.02 (±0.17)
2	11.11 (±0.39)	6.81 (±0.27)	11.37 (±0.55)	6.23 (±0.27)
3	2.31 (±0.19)	0.90 (±0.03)	2.70 (±0.30)	0.76 (±0.03)
4	4.07 (±0.16)	1.49 (±0.11)	5.73 (±0.31)	2.53 (±0.17)
5	10.06 (±0.50)	4.17 (±0.22)	11.30 (±0.41)	5.47 (±0.33)
6	13.84 (±0.73)	9.56 (±0.31)	8.50 (±0.33)	4.91 (±0.18)
7	4.25 (±0.31)	2.08 (±0.20)	3.62 (±0.23)	1.62 (±0.05)
8	11.53 (±0.48)	5.68 (±0.19)	12.90 (±0.45)	6.94 (±0.32)
Photofrin ^{®c}	>41	4.3 (±0.2)	–	–
Cisplatin ^d	71.3(±2.9)	68.7(± 3.4)	–	–

^a The IC₅₀ values correspond to 24 h incubation in dark.

^b The IC₅₀ values correspond to 4 h incubation in dark followed by photo-exposure to visible light (400–700 nm, 10 J cm⁻²).

^c The IC₅₀ values (633 nm excitation; fluence rate: 5 J cm⁻²) of Photofrin[®] are taken from reference No. 83 (converted to μM using the approximate molecular weight of Photofrin[®] = 600 g M⁻¹).

^d The IC₅₀ values are taken from reference No. 37.

3.7. Cellular localization

The delivery of a therapeutic agent to the targeted cellular organelles is the key to the success of such compounds [85–87]. Incorporation of a fluorescent naphthyl moiety in complex **4** was primarily aimed to study the uptake and localization of the complex in the cellular organelles in HeLa cells from microscopic images. The cells were treated with complex **4** for different time intervals and observed by fluorescence microscopy (Fig. 12). It was observed that at 1.0 h time point the complex is primarily in the cytoplasm with minor accumulation in the nucleus (panel (a), Fig. 12). After 2.0 h the complex moves from the cytoplasm and predominantly localizes in the nucleus of the HeLa cells with reduced blue fluorescence from the cytoplasm (panel (e) in Fig. 12). At 4 h the intensity of fluorescence further increases indi-

cating that the complex primarily localizes in the nucleus at that time (panel (i) in Fig. 12). The cells were stained for the nucleus with propidium iodide (PI) which stains the nucleic acids and in the presence of RNase degrades the cellular RNA (panels (b), (f) and (j) in Fig. 12). The cells are treated with RNase-A which degrades the cellular RNA to avoid PI staining of the RNA in the cytoplasm. On merging the blue fluorescence of **4** and red fluorescence of PI, the panels (g) and (k) in Fig. 12 turned pink in colour at the position of the nucleus indicating nuclear localization of complex **4**. The bright field images confirm that the fluorescence images are from the cellular organelles and are not artifacts (Fig. 12, panels (d), (h) and (l)). Further, to confirm whether the fluorescence is due to sticking of the compound on the cell or nuclear membrane, optical sectioning of the cells was done to analyze the cells in 3D. The cells, sectioned along the z-axis, at intervals of 1 μm, clearly

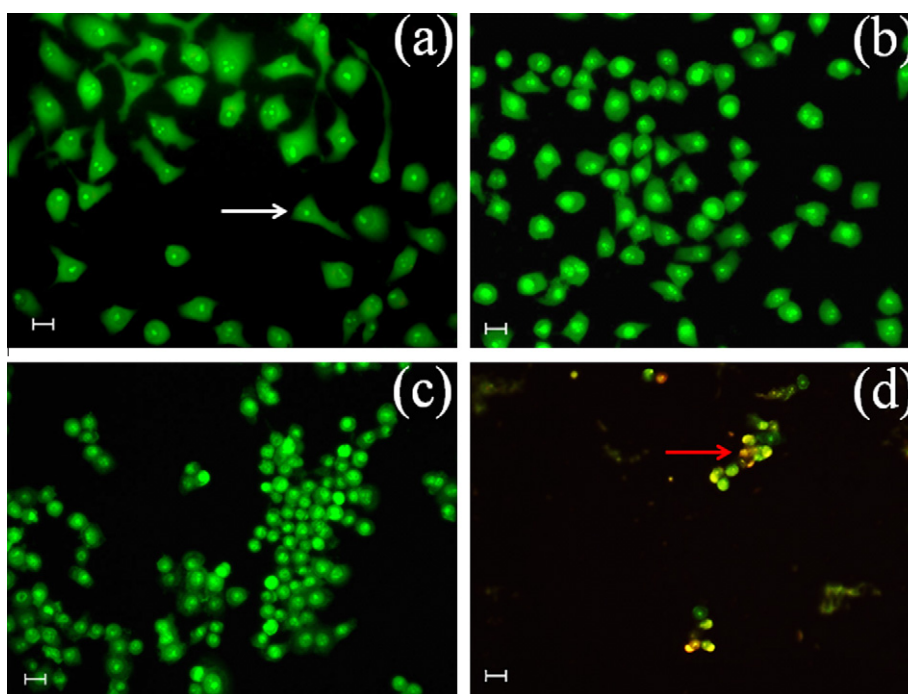


Fig. 11. Acridine orange (white arrow)/ethidium bromide (red arrow) (AO/EB) dual staining of HeLa cells treated with complex **3** (5 μM) to study the nuclear morphology. Panels (a) and (b) correspond to the cells treated with only DMSO in dark and light, respectively; panel (c) corresponds to the cells treated with complex **3** in dark and panel (d) corresponds to the cells treated with complex **3** and irradiated with visible light (400–700 nm, 10 J cm⁻²). The scale bar in the panels corresponds to 20 μm. (Colour online.)

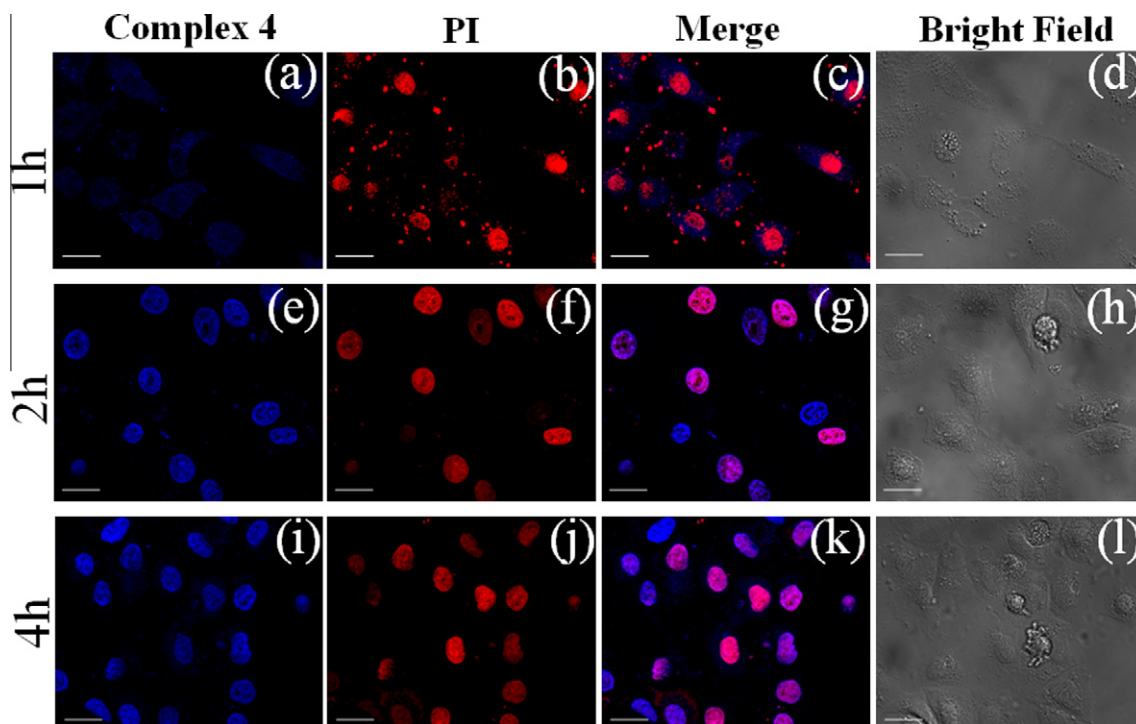


Fig. 12. A time-course collection of fluorescence microscopic images of HeLa cells treated with complex **4** (5 μM) and propidium iodide (PI). Panels (a), (e) and (i) correspond to the blue emission of complex **4** and the respective images were taken after 1, 2 and 4 h. Panels (b), (f) and (j) correspond to the red emission of PI. Panels (c), (g) and (k) are the merged images of the first two panels. Panels (d), (h) and (l) are the bright field images. The scale bar in panel (a) corresponds to 20 μM .

showed blue fluorescence in the whole nucleus and not an artifact due to deposition of the complex on cell or nuclear membrane.

4. Conclusions

Ternary copper(II) complexes containing ferrocene-conjugated L-tyrosine reduced Schiff base and phenanthroline bases were synthesized, characterized and their photo-induced DNA cleavage activity, cytotoxicity and cellular localization studied. The complexes are designed to serve the dual purpose as DNA binder and photosensitizer. The effect of the ferrocenyl moiety is observed from the cytotoxicity of the ferrocenyl complexes. The ferrocenyl complexes showed less undesirable hydrolytic cleavage of DNA than the Ph-Tyr complexes. The complexes exhibit efficient groove binding propensity to ct-DNA with partial intercalative binding mode of the dppz complexes. The complexes show moderate chemical nuclease activity in the presence of both reducing (GSH) and oxidizing (H_2O_2) agents involving both the metal centers. The complexes displaying significant photo-induced DNA cleavage activity in blue, green and red light are remarkably photo-cytotoxic towards cervical and breast cancer cells. Significant photodynamic effect on nuclear morphology is observed when HeLa cells are treated with complex **3** and subsequently photo-irradiated in comparison to the non-irradiated samples. The fluorescence emission of the nip complex **4** bearing a naphthyl moiety is successfully used for cellular imaging which shows nuclear localization of the complex in the HeLa cells. The results showing remarkable photocytotoxicity of the ferrocene-conjugates having copper(II) centre are of significance in the virtually unexplored chemistry of bioorganometallics in PDT.

Acknowledgements

We thank the Department of Science and Technology (DST), Government of India, for financial support (SR/S5/MBD-02/2007).

We are thankful to the DST for a CCD diffractometer facility, Alexander von Humboldt Foundation, Germany, for donation of an electroanalytical system. ARC thanks DST for J. C. Bose national fellowship. TKG and SG thank CSIR, New Delhi, for research fellowships.

Appendix A. Supplementary data

CCDC 878189 and 878190 contains the supplementary crystallographic data for complexes **5a** and **6**. These data can be obtained free of charge via <http://www.ccdc.cam.ac.uk/conts/retrieving.html>, or from the Cambridge Crystallographic Data Centre, 12 Union Road, Cambridge CB2 1EZ, UK; fax: (+44) 1223 336 033; or e-mail: deposit@ccdc.cam.ac.uk. Supplementary data associated with this article can be found, in the online version, at <http://dx.doi.org/10.1016/j.poly.2012.06.018>.

References

- [1] N.J. Wheate, S. Walker, G.E. Craig, R. Oun, Dalton Trans. 39 (2010) 8113.
- [2] H.-K. Liu, P.J. Sadler, Acc. Chem. Res. 44 (2011) 349.
- [3] A. Bergamo, G. Sava, Dalton Trans. 40 (2011) 7817.
- [4] T.W. Hambley, Science 318 (2007) 1392.
- [5] A. Bergamo, C. Gaiddon, J.H.M. Schellens, J.H. Beijnen, G. Sava, J. Inorg. Biochem. 106 (2012) 90.
- [6] L. Kelland, Nat. Rev. Cancer 7 (2007) 573.
- [7] D. Wang, S.J. Lippard, Nat. Rev. Drug Disc. 4 (2005) 307.
- [8] K.S. Lovejoy, S.J. Lippard, Dalton Trans. (2009) 10651.
- [9] L. Ronconi, D. Fregona, Dalton Trans. (2009) 10670.
- [10] S. Dhar, N. Kolishetti, S.J. Lippard, O.C. Farokhzad, Proc. Natl. Acad. Sci. U. S. A. 108 (2011) 1850.
- [11] S. Dhar, W.L. Daniel, D.A. Giljohann, C.A. Mirkin, S.J. Lippard, J. Am. Chem. Soc. 131 (2009) 14652.
- [12] F.S. Mackay, N.J. Farrer, L. Salassa, H.-C. Tai, R.J. Deeth, S.A. Moggach, P.A. Wood, S. Parsons, P.J. Sadler, Dalton Trans. (2009) 2315.
- [13] N.J. Farrer, J.A. Woods, L. Salassa, Y. Zhao, K.S. Robinson, G. Clarkson, F.S. Mackay, P.J. Sadler, Angew. Chem. Int. Ed. 49 (2010) 8905.
- [14] S.J. Berners-Price, Angew. Chem. Int. Ed. 50 (2011) 804.
- [15] R. Bonnett, Chemical Aspects of Photodynamic Therapy, Gordon & Breach, London, U.K., 2000.

- [16] M. Ethirajan, Y. Chen, P. Joshi, R.K. Pandey, *Chem. Soc. Rev.* 40 (2011) 340.
- [17] A.M. Bugaj, *Photochem. Photobiol. Sci.* 10 (2011) 1097.
- [18] M. Korbelik, *Photochem. Photobiol. Sci.* 10 (2011) 664.
- [19] N.L. Fry, P.K. Mascharak, *Acc. Chem. Res.* 44 (2011) 289.
- [20] D. Crespy, K. Landfester, U.S. Schubert, A. Schiller, *Chem. Commun.* 46 (2010) 6651.
- [21] G.-J. Chen, X. Qiao, J.-L. Tian, J.-Y. Xu, W. Gu, X. Liu, S.-P. Yan, *Dalton Trans.* 39 (2010) 10637.
- [22] M. Ochsner, *J. Photochem. Photobiol.*, B 32 (1996) 3.
- [23] S.I. Moriwaki, J. Misawa, Y. Yoshinari, I. Yamada, M. Takigawa, Y. Tokura, *Photodermatol. Photoimmunol. Photomed.* 17 (2001) 241.
- [24] N.J. Farrer, L. Salassa, P.J. Sadler, *Dalton Trans.* (2009) 10690.
- [25] A.D. Ostrowski, P.C. Ford, *Dalton Trans.* (2009) 10660.
- [26] H.T. Chifotides, K.R. Dunbar, *Acc. Chem. Res.* 38 (2005) 146.
- [27] U. Basu, I. Khan, A. Hussain, P. Kondaiah, A.R. Chakravarty, *Angew. Chem. Int. Ed.* 51 (2012) 2658.
- [28] U. Schatzschneider, *Eur. J. Inorg. Chem.* (2010) 1451.
- [29] F.S. Mackay, J.A. Woods, P. Heringová, J. Kašpárková, A.M. Pizarro, S.A. Moggach, S. Parsons, V. Brabec, P.J. Sadler, *Proc. Natl. Acad. Sci. U.S.A.* 104 (2007) 20743.
- [30] T. Gianferrara, I. Bratsos, E. Alessio, *Dalton Trans.* (2009) 7588.
- [31] A.A. Holder, D.F. Zigler, M.T. Tarrago-Trani, B. Storrie, K.J. Brewer, *Inorg. Chem.* 46 (2007) 4760.
- [32] G.S. Smith, B. Therrien, *Dalton Trans.* 40 (2011) 10793.
- [33] R.N. Garner, J.C. Gallucci, K.R. Dunbar, C. Turro, *Inorg. Chem.* 50 (2011) 9213.
- [34] L.E. Joyce, J.D. Aguirre, A.M. Angeles-Boza, A. Chouai, P.K.-L. Fu, K.R. Dunbar, C. Turro, *Inorg. Chem.* 49 (2010) 5371.
- [35] A.M. Angeles-Boza, P.M. Bradley, P.K.-L. Fu, M. Shatruk, M.G. Hilfinger, K.R. Dunbar, C. Turro, *Inorg. Chem.* 44 (2005) 7262.
- [36] B. Maity, M. Roy, B. Banik, R. Majumdar, R.R. Dighe, A.R. Chakravarty, *Organometallics* 29 (2010) 3632.
- [37] S. Saha, D. Mallick, R. Majumdar, M. Roy, R.R. Dighe, E.D. Jemmis, A.R. Chakravarty, *Inorg. Chem.* 50 (2011) 2975.
- [38] B. Maity, M. Roy, S. Saha, A.R. Chakravarty, *Organometallics* 28 (2009) 1495.
- [39] B. Maity, S. Gadadhar, T.K. Goswami, A.A. Karande, A.R. Chakravarty, *Dalton Trans.* 40 (2011) 11904.
- [40] T.K. Goswami, M. Roy, M. Nethaji, A.R. Chakravarty, *Organometallics* 28 (2009) 1992.
- [41] A. Nguyen, S. Top, A. Vessieres, P. Pigeon, M. Huche, E.A. Hillard, G. Aouen, *J. Organomet. Chem.* 692 (2007) 1219.
- [42] E. Hillard, A. Vessières, L. Thouin, G. Jaouen, C. Amatore, *Angew. Chem. Int. Ed.* 45 (2006) 285.
- [43] G. Gasser, I. Ott, N. Metzler-Nolte, *J. Med. Chem.* 54 (2011) 3.
- [44] D. Dive, C. Biot, *ChemMedChem* 3 (2008) 383.
- [45] C.G. Hartinger, P.J. Dyson, *Chem. Soc. Rev.* 38 (2009) 391.
- [46] P.J. Dyson, G. Sava, *Dalton Trans.* (2006) 1929.
- [47] S. Chatterjee, S. Kundu, A. Bhattacharyya, C.G. Hartinger, P.J. Dyson, *J. Biol. Inorg. Chem.* 13 (2008) 1149.
- [48] B. Balaji, B. Banik, P.K. Sasmal, B. Maity, R. Majumdar, R.R. Dighe, A.R. Chakravarty, *Eur. J. Inorg. Chem.* (2012) 126.
- [49] B. Banik, P.K. Sasmal, S. Roy, R. Majumdar, R.R. Dighe, A.R. Chakravarty, *Eur. J. Inorg. Chem.* (2011) 1425.
- [50] P.K. Sasmal, S. Saha, R. Majumdar, R.R. Dighe, A.R. Chakravarty, *Chem. Commun.* (2009) 1703.
- [51] P.K. Sasmal, R. Majumdar, R.R. Dighe, A.R. Chakravarty, *Dalton Trans.* 39 (2010) 7104.
- [52] P.K. Sasmal, S. Saha, R. Majumdar, R.R. Dighe, A.R. Chakravarty, *Inorg. Chem.* 49 (2010) 849.
- [53] F. Schmitt, P. Govindaswamy, G. Süß-Fink, W.H. Ang, P.J. Dyson, L. Juillerat-Jeanneret, B. Therrien, *J. Med. Chem.* 51 (2008) 1811.
- [54] F. Schmitt, P. Govindaswamy, O. Zava, G. Süß-Fink, L. Juillerat-Jeanneret, B. Therrien, *J. Biol. Inorg. Chem.* 14 (2009) 101.
- [55] D.D. Perrin, W.L.F. Armarego, D.R. Perrin, *Purification of Laboratory Chemicals*, Pergamon Press, Oxford, 1980.
- [56] J.E. Dickeson, L.A. Summers, *Aust. J. Chem.* 23 (1970) 1023.
- [57] E. Amouyal, A. Homsí, J.-C. Chambron, J.-P. Sauvage, *J. Chem. Soc., Dalton Trans.* (1990) 1841.
- [58] S.S. Bhat, A.A. Kumbhar, H. Heptullah, A.A. Khan, V.V. Gobre, S.P. Gejji, V.G. Puranik, *Inorg. Chem.* 50 (2011) 545.
- [59] S.C. Sahoo, M. Ray, *Dalton Trans.* (2009) 3230.
- [60] D.F. Evans, *J. Chem. Soc.* (1959) 2003.
- [61] D.F. Evans, T.A. James, *J. Chem. Soc., Dalton Trans.* (1979) 723.
- [62] N. Walker, D. Stuart, *Acta Crystallogr., Sect. A* 39 (1983) 158.
- [63] G.M. Sheldrick, *Acta Cryst. A* 64 (2008) 112.
- [64] C.K. Johnson, ORTEP-III, Report ORNL-5138; Oak Ridge National Laboratory, Oak Ridge, TN, 1976.
- [65] L.J. Farrugia, *J. Appl. Cryst.* 30 (1997) 565.
- [66] T.K. Goswami, B.V.S.K. Chakravarthi, M. Roy, A.A. Karande, A.R. Chakravarty, *Inorg. Chem.* 50 (2011) 8452.
- [67] T. Mosmann, *J. Immunol. Methods.* 65 (1983) 55.
- [68] J.E. Coligan, A.M. Kruisbeck, D.H. Margulies, E.M. Shevach, W. Strober, in: R. Coico (Ed.), *Related Isolation Procedures and Functional Assay, Current Protocols in Immunology*, John Wiley & Sons, Inc., New York, 1995. p 3.17.1.
- [69] J.L. McClintock, B.P. Ceresa, *Invest. Ophthalmol. Vis. Sci.* 51 (2010) 3455.
- [70] B.J. Hathaway, A.E. Underhill, *J. Chem. Soc.* (1961) 3091.
- [71] A.K. Patra, M. Nethaji, A.R. Chakravarty, *Dalton Trans.* (2005) 2798.
- [72] W.J. Geary, *Coord. Chem. Rev.* 7 (1971) 81.
- [73] Y.S. Sohn, D.N. Hendrickson, H.B. Gray, *J. Am. Chem. Soc.* 933 (1971) 3603.
- [74] A.W. Addison, T.N. Rao, J.V. Reedijk, G.C. Verschoor, *J. Chem. Soc., Dalton Trans.* (1984) 1349.
- [75] A.M. Pyle, J.P. Rehmann, R. Meshoyrer, C.V. Kumar, N.J. Turro, J.K. Barton, *J. Am. Chem. Soc.* 111 (1989) 3051.
- [76] A. Hussain, D. Lahiri, M.S.A. Begum, S. Saha, R. Majumdar, R.R. Dighe, A.R. Chakravarty, *Inorg. Chem.* 49 (2010) 4036.
- [77] T.K. Goswami, S. Gadadhar, M. Roy, M. Nethaji, A.A. Karande, A.R. Chakravarty, *Organometallics* 31 (2012) 3010.
- [78] M. Cory, D.D. Mckee, J. Kagan, D.W. Henry, J.A. Miller, *J. Am. Chem. Soc.* 107 (1985) 2528.
- [79] K.E. Reinert, *Biochim. Biophys. Acta* 319 (1973) 135.
- [80] P.J. Higgins, A.M. Gellert, *Bioorg. Med. Chem. Lett.* 19 (2009) 1614.
- [81] S.R. Logan, *Can. J. Chem.* 69 (1991) 540.
- [82] G. Tabbi, C. Cassino, G. Cavigliolo, D. Colangelo, A. Ghiglia, I. Viano, D. Osella, *J. Med. Chem.* 45 (2002) 5787.
- [83] E. Delaey, F. Van Larr, D. De Vos, A. Kamuhabwa, P. Jacobs, P. De Witte, *J. Photochem. Photobiol. B* 55 (2000) 27.
- [84] N.J. Wheate, C.R. Brodie, J.G. Collins, S. Kemp, J.R. Aldrich-Wright, *Mini Rev. Med. Chem.* 7 (2007) 627.
- [85] T. Storr, K.H. Thompson, *C. Orvig, Chem. Soc. Rev.* 35 (2006) 534.
- [86] K.H. Thompson, C. Orvig, *Dalton Trans.* (2006) 761.
- [87] N. Fozia, A. Wüstholtz, R. Kinscherf, N. Metzler-Nolte, *Angew. Chem. Int. Ed.* 44 (2005) 2429.